Liang, Yunpei; Tan, Youting; Wang, Fakai; Luo, Yongjiang; Zhao, Zhiqiang

Article

Improving permeability of coal seams by freeze-fracturing method: The characterization of pore structure changes under low-field NMR

Energy Reports

Provided in Cooperation with:
Elsevier

Suggested Citation: Liang, Yunpei; Tan, Youting; Wang, Fakai; Luo, Yongjiang; Zhao, Zhiqiang (2020) : Improving permeability of coal seams by freeze-fracturing method: The characterization of pore structure changes under low-field NMR, Energy Reports, ISSN 2352-4847, Elsevier, Amsterdam, Vol. 6, pp. 550-561, https://doi.org/10.1016/j.egyr.2020.02.033

Energy Reports 6 (2020) 550–561

Contents lists available at ScienceDirect

Energy Reports

journal homepage: www.elsevier.com/locate/egyr

Research paper

Improving permeability of coal seams by freeze-fracturing method: The characterization of pore structure changes under low-field NMR

Yunpei Liang [a,b], Youting Tan [a,b], Fakai Wang [a,b], Yongjiang Luo [a,b,*], Zhiqiang Zhao [c]

[a] State Key Laboratory of Coal Mine Disaster Dynamics and Control, Chongqing University, Chongqing 400044, China
[b] College of Resources and Environmental Science, Chongqing University, Chongqing 400044, China
[c] China Coal Technology and Engineering Group Chongqing Research Institute, Chongqing, 400039, China

ARTICLE INFO

Article history:
Received 5 December 2019
Received in revised form 22 February 2020
Accepted 26 February 2020
Available online xxxx

Keywords:
Freeze-fracturing
Coal pore structure
Permeability
Nuclear magnetic resonance

ABSTRACT

The method of improving permeability of coal seams by freeze-fracturing is presented to accelerate the diffusion of coalbed gas into exploited wells. The pore structure of coal sample changes caused by freeze-fracturing were characterized by nuclear magnetic resonance (NMR) and scanning electron microscopy (SEM), and a permeability-calculation model was employed to estimate the permeability of coal sample. The pore size distribution, porosity, and permeability of coal before and after freezing were analyzed. Results show that freeze-fracturing can complicate the coal pore structure, and its complexity is positively correlated with the freezing temperature and coal moisture content. The main manifestation is the growth and expansion of coal pores, with higher pore connectivity, generation of gas seepage pores with pore diameter > 100 nm, and expansion of original pores into larger ones. By comparing the connectivity and seepage space of the pore structure of coal before and after freezing, it is concluded that freeze-fracturing can promote the coal seam permeability significantly, which is beneficial for the exploitation of coalbed gas.

1. Introduction

As a byproduct of coal seams, coalbed gas has attracted worldwide attention as an unconventional natural gas source since the late 20th century. Its resource is distributed across 74 countries, with estimated reserves of 240 $\times$ 10^{12} m^3 at the depth of less than 2000 m, which is more than twice the proven reserves of conventional natural gas (Dai et al., 2018). Approximately 80% to 99% of the coalbed gas is methane; other gases, such as nitrogen, carbon dioxide, and hydrogen sulfide are also present. Most of the coalbed gas is in the adsorption state in which it adheres to the coal surface owing to temperature, initial gas pressure and coal composition and pore structure (Cai et al., 2019; Sun et al., 2019a,b); in the free state, the gas dissociates from coal pores owing to gas flowability (Ko, 2018). In underground coal mining, coalbed gas may trigger mine disasters, owing to its movement and emission, which results in outbursts and explosions (Goraya et al., 2019; Liang et al., 2019). Therefore, coalbed gas extraction before coal mining can not only increase available gas resources, but also improve underground mining safety (Deng et al., 2013; Yoon et al., 2019).

Coal permeability, which is closely related to coal pore structure, is a key parameter in coalbed methane production (Shi et al., 2018). However, it must satisfy certain requirements to be economical viable in the extraction of coalbed gas. The low permeability of partial coal seams and high affinity for gas adsorption necessitated many attempts to promote the development and expansion of fractures in coal and improve the permeability of coal seams (Javadpour et al., 2015). Hydraulic fracturing, which has been developed in the oil and gas industry, is typically used to extend the width, length, and connectivity of natural fracture systems in coal seams. However, using hydraulic fracture fluids with additives is not environmentally desirable, because it increases the drain cost, leads groundwater pollution, and causes potential well failure and even earthquakes when used in deep-well injections (Li et al., 2019; Chen et al., 2020). Furthermore, hydraulic fracturing method employed in oil and gas industry has low efficiency for dealing with low-strength coals (Sun et al., 2019b; Zhao et al., 2019). New hydraulic fracturing fluids such as liquid nitrogen and liquid carbon dioxide are safer than conventional fracturing fluids, and can significantly improve coal permeability, but they increase the gas mixture in the coalbed gas, which in turn increases the cost of gas separation (Cai et al., 2018; Wen et al., 2019). Therefore, new approaches to permeability enhancement in coal seams are an essential requirement.

* Corresponding author at: State Key Laboratory of Coal Mine Disaster Dynamics and Control, Chongqing University, Chongqing 400044, China.
E-mail address: luoyj16@cqu.edu.cn (Y. Luo).

https://doi.org/10.1016/j.egyr.2020.02.033

Freeze-fracturing can change the coal pore structure and increase the seepage space, which could enhance the coal permeability without the above-mentioned problems (Li et al., 2016; Wang et al., 2019). In previous studies, low-temperature media for coal fracturing mainly considered liquid nitrogen and liquid carbon dioxide (Xu et al., 2017; Zhang et al., 2018a). Zhai et al. (2016) used liquid nitrogen for freezing–thawing (F–T) fracturing and demonstrated that the stress generated by the F–T cycle is beneficial for fissure generation and permeability improvement. Sun et al. (2018) studied the evolution of the coal pore structure for different freezing temperatures, using the F–T cycle method, and concluded that temperature reduction is beneficial for increasing the pore growth and seepage space. Ni et al. (2015) analyzed the change characteristics of coal seams after carbon dioxide injection, using an electron microscope and a permeability tester. Zhai et al. (2017) used nuclear magnetic resonance (NMR) to determine the effect of F–T cycles on the coal porosity with different cycle number and stress values. Yang and Bi (2018) used low-field NMR to determine the effect of ultra-low temperatures (100 °C, −196 °C) on the coal pore structure, and demonstrated that low temperatures are beneficial for increasing the pore size and permeability, while high temperatures are adverse to those. Yin et al. (2018) studied changes in coal pore structure and permeability, for different moisture content levels, by using cryogenic fracturing of liquid nitrogen. These studies rarely addressed the effect of low-temperature fracturing with pure water on the coal pore structure. In addition, the above-mentioned research mainly focused on damage characteristics of pore structures under repeated F–T cycles; consequently, they provide only limited insights into the characteristics and changes of the coal pore structure under rapid freeze-fracturing.

This paper reports the effects of different freezing temperatures and coal moisture contents on the coal pore structure through the direct freeze-fracturing effect. The pore structure characteristics of the studied coal samples, before and after freezing, were observed using scanning electron microscopy (SEM), NMR, and the permeability model calculations. The T_2 distribution spectrum is discussed to analyze pore development and expansion, including the number of pores, pore size, porosity and permeability. The results of this study are likely to provide experimental data for freezing seepage studies of coal seams.

2. Theoretical background on NMR

Coal seams have fragile, compressible and complex pore structures, which make highly heterogeneous. The molecular diameter of gas is 0.414 nm, and exists in coal pore with pore size larger than 10 nm by adsorption or dissociation (Zhang et al., 2018b; Zheng et al., 2018). The NMR aperture measurement ranges from 10^{-3} to 10^5 nm with high efficiency and nondestructive property of specimens, is widely used for analyzing pore distributions and pore structures in coal reservoirs. NMR refers to the collective response of atomic nuclei to a radio frequency in the presence of a magnetic field, and due to the coal skeleton has no signal, this method normally measures the relaxation characteristics of fluids in coal pores (Brown and Fatt, 1956). The time required for the transverse magnetic field intensity to decrease to 37% of its original value (M_0) is called the relaxation time (T_2) (Xie et al., 2015), which is an important factor because the different substances have different T_2, and the same substance in different factors has different T_2 (Liu et al., 2019). The relaxation characteristics in the presence of a magnetic field can be categorized into three types: (1) free relaxation, (2) surface relaxation, and (3) diffusion relaxation; all of these processes affect T_2 (Liu and Wu, 2017; Shikhov et al., 2018). For coal seams, the free relaxation and diffusion relaxation of fluids are much weaker than the surface relaxation; thus, typically, only the effect of the surface relaxation on T_2 is considered (Zhao et al., 2018; Chen et al., 2019).

In addition, NMR can detect hydrogen, which helps it distinguish between volumetric fluids and surface fluids in coal samples (Guo et al., 2007; Guo and Kantzas, 2009). When there is no signal in the coal skeleton and surface fluid that includes the adsorbed gas and moisture, NMR detects the volumetric fluid in the coal pores, which contain free gas and free water. When a coal pore is filled with a volumetric fluid, the fluid volume is equal to the pore volume; thus, the porosity measured using NMR can reflect the actual porosity of coal. The Carr–Purcell–Meiboom–Gill (CPMG) pulse sequences of fully water-saturated coal samples are tested to obtain the attenuation curves of spin echo series, and by fitting the sum of curves to the attenuation amplitude of spin echo strings the attenuation constants for different pore sizes can be derived; a superposition of these constitutes the T_2 distribution spectrum.

The expression for T_2 and pore size, when only the effect of the surface relaxation is considered, is as follows:

$$\frac{1}{T_2} = \rho\left(\frac{S}{V}\right) = F_s\left(\frac{\rho}{\gamma}\right) \tag{1}$$

T_2—relaxation time, ms;
ρ—surface relaxation strength, m/ms;
S—pore surface area, m^2;
V—pore volume, m^3;
F_s—pore geometry factor (spherical pore, $F_s = 3$; columnar pore, $F_s = 2$; fissure, $F_s = 1$) (Yao et al., 2010; Xie et al., 2015);
γ—pore size, m.

Based on Eq. (1), we can write:

$$\gamma = T_2 F_s \rho \tag{2}$$

According to Eq. (2), T_2 is positively correlated with the coal pore size, and the amplitude of the T_2 curve is positively correlated with pore quantity; thus, the T_2 distribution can be used for computing the coal physical parameters, as well as the connectivity and distribution of various pores in coal.

3. Experiments

3.1. Experimental apparatus

The experimental apparatus employed in this study included a temperature frequency conversion control system, an NMR test system, and an SEM system (Fig. 1). The temperature frequency conversion control system comprised of a temperature control system and a data acquisition system, in which the data acquisition system collected parameters and the temperature control system was realized as a thermostat air bath with a range of −50 °C to 50 °C, deviation of $\leq \pm 1$ °C, and temperature fluctuation of ±0.5 °C. The NMR test system called Macro MR12-150H-I, manufactured by Suzhou Niumag Analytical Instrument Corporation, was composed of an NMR core analyzer, an imager, a high-temperature and high-pressure displacement probe, and other related equipment. For the NMR core analyzer, the magnetic field intensity was 0.3 ± 0.05 T, the frequency range of radio frequency pulses was 2–30 MHz, and the peak output was above 300 W (Tables 1 and 2). All data conform to the national standard of "Specification for normalization measurement of core NMR parameter in laboratory (SY/T 6490-2007)". The SEM model was EVO LS10, manufactured by British Carl Zeiss Microscopy Ltd; this SEM was used to generate coal pore images. The studio size was 310 mm (Φ) × 220 mm (h), the environmental vacuum mode resolution was 3.0 nm @ 30 kV, the acceleration voltage was 0.2–30 kV, the amplification factor was 7–1000000, and the system was controlled by the Smart SEM operating system running on Windows XP.

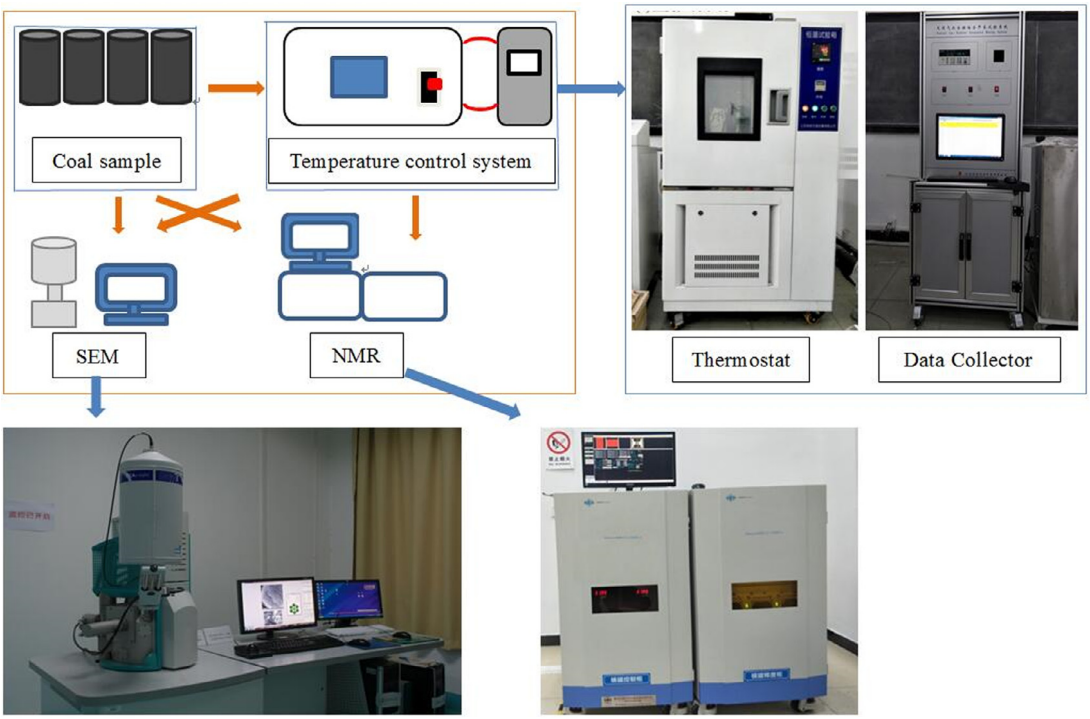

Fig. 1. Experimental apparatus.

Table 1
The parameters of CPMG sequence.

System parameter	Numerical value
Magnet temperature (°C)	25
Scan time (ms)	0.181
SF (MHz)	12
O1 (Hz)	682 035.1
RFD (ms)	0.02
P1 (μs)	3.8
P2 (μs)	10.2
TD	99 980
TE (ms)	0.5
TW (ms)	500
RG1	20.0
NS	8
NECH	5000

(*SF*- Spectrometer Frequency, *O1*- Frequency offset 1, *RFD*- Sampling time, *P1*- 90° pulse length, *P2*- 180° pulse length, *TD*- Time domain, *TE*- inter-echo spacing time, *TW*- Waiting time, *RG1*- Analog Gain, *NS*- Number of repeated sampling times, *NECH*- Echo number.)

Table 2
The parameters of imaging system.

System parameter	Numerical value
SF (MHz)	12
O1 (Hz)	671 869.0
FOV (mm)	150
Resolution ratio (Linear)	0.999
Signal to noise ratio (ppm)	100
GxOffset	20
GyOffset	−5
GzOffset	−65
RFA90	3.7
RFA180	7.6

(*SF*-Spectrometer frequency, *O1* -Frequency offset 1, *FOV* -Field of view, GxOffset-Gradient coil X, GyOffset-Gradient coil Y, GzOffset-Gradient coil Z, *RFA90* -90° pulse amplitude, *RFA180* -180° pulse amplitude.)

3.2. Coal sample preparation

Coal samples were high-rank anthracite having a primary structure, extracted from the Guizhou mine. To ensure experimental accuracy, all the samples were extracted from the same place by coal machine, and using coal cutter to make their dimensions be 50 mm × 100 mm. According to the National Coal Industry Standard, the coal samples were screened using the Tektronix TBS 1202B-EDU oscilloscope to have the ultrasonic wave velocity physical property test, and their industrial analysis indices were determined (Fig. 2, Table 3). Three types of test samples were considered: (1) natural coal, (2) dry coal, and (3) water-saturated coal. The natural coal samples were obtained by drilling boreholes without artificial processing. The coal samples were dried by using the vacuum dryer until the rate of their weight change dropped under 0.1 g/h. The steps to obtain the water-saturated coal samples are as follows: the coal samples are completely dried and weighed at room temperature firstly; Second, samples were saturated in a vacuum water-saturated device at the vacuum pressure of −0.1 MPa, for 12 h to ensure that the rate of their weight change dropped under 0.1 g/h; Last, according to "Method of core routine analysis (SY-T 5336-1996)", bring the weight of coal samples between dry and water-saturated into the formula, and if the error of the result is within 5%, it is proved to be completely saturated.

3.3. Experimental procedure

Aimed at studying the pore structure characteristics and the evolution of coal porosity with freezing, the main test factors in our experiments were water and temperature. Based on these, the experiments were divided into two sets, for characterizing the freeze-fracturing effect on the coal samples with different freezing temperatures and moisture content (Table 4). For case I, 4 groups (8 specimens) of water-saturated coal samples were selected for performing low-field NMR tests, corresponding to 4 freezing temperatures (10 °C, 0 °C, −10 °C, and −20 °C). For case II;, 3 groups (6 specimens) of coal samples with different moisture

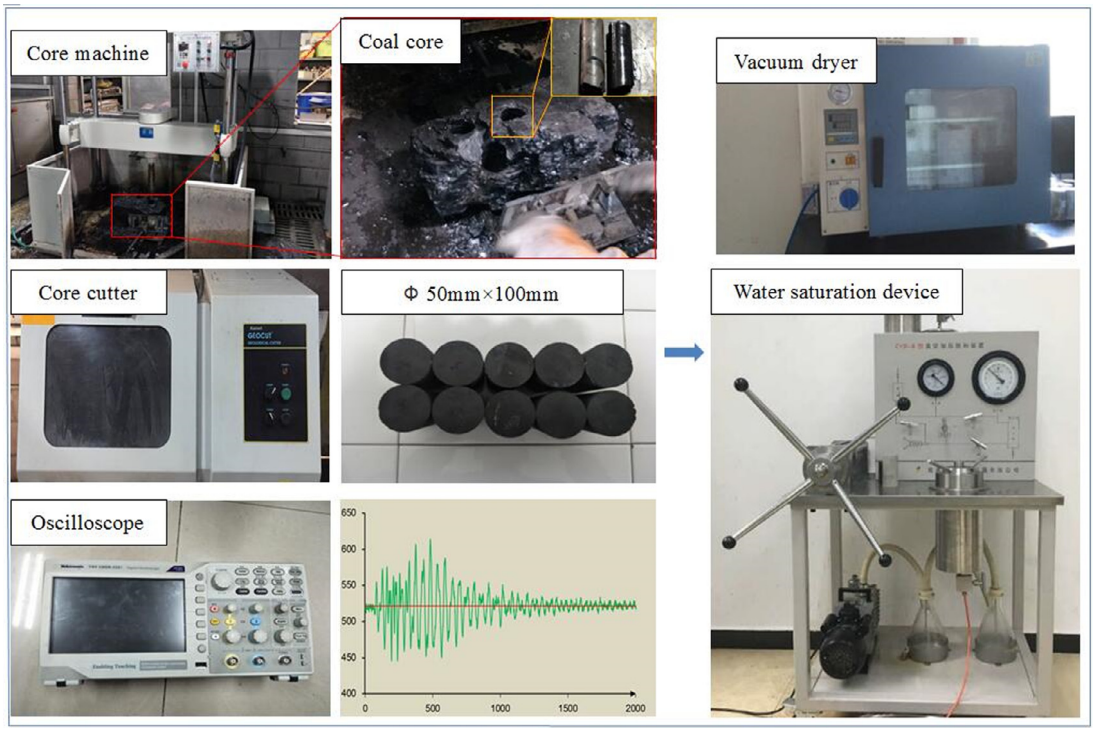

Fig. 2. Coal sample preparation. (Drilling→Cutting samples→Oscilloscope testing→dry or saturated samples.)

Table 3
Coal macerals and industrial analysis indicators.

Coal macerals (%)				Industrial analysis (%)				*TRD* (g/cm^3)	*ARD* (g/cm^3)
V	*I*	*E*	*M*	M_{ad}	A_{ad}	V_{daf}	F_{Cad}		
84.5	12.5	1.6	1.4	1.01	1.95	8.51	88.62	1.51	1.48

(*V*- vitrinite, *I*- Inertinite, *E*- exinite, *M*- mineral, M_{ad}- air drying base moisture content, A_{ad}- air drying base ash content, V_{daf}- dry ashless base volatile content, F_{Cad}- fixed carbon content, *TRD*- true relative density, *ARD*- apparent relative density.)

Table 4
Experimental conditions and parameters.

Case	Coal sample	Freezing temperature	Water content of coal
Case 1–1	Water-saturated	10 °C	4.45%
Case 1–2	Water-saturated	0 °C	4.45%
Case 1–3	Water-saturated	−10 °C	4.45%
Case 1–4	Water-saturated	−20 °C	4.45%
Case 2–1	Dry	−20 °C	0%
Case 2–2	Natural	−20 °C	1.90%
Case 2–3	Water-saturated	−20 °C	4.45%

content (4.45%, 1.90%, and 0%) were selected to conduct low-field NMR tests at the freezing temperature of −20 °C. In both cases, we used NMR imaging, electron microscopy scanning, and oscilloscope-based observations, for imaging and wave velocity analysis of the coal samples before and after freezing, in order to observe changes in the coal pore structure.

4. Results and discussion

Coal pore characteristics mainly include pore size distribution, porosity and permeability. Here, we will focus on these four features, to discuss changes in the coal pore characteristics with freezing temperature and moisture content, before and after freezing.

4.1. Pore characteristics changes in water-saturated coal samples with freezing temperature

Fig. 3 shows the water distribution in water-saturated coal samples before and after freezing; these water distributions were obtained from top to bottom by using magnetic resonance imaging (MRI). In Fig. 3, the blue area corresponds to the coal matrix while other colors correspond to the water dispersed in coal; the moisture content increases as the area color changes from blue to red. The MRI images of the water-saturated coal samples before freezing are uniform, which indicates that the water distribution inside the coal samples is relatively uniform. Meanwhile, the MRI images of the water-saturated coal samples after freezing feature darker areas with irregular bands, which indicates water diffusion during the freezing process. This suggests the presence of more complicated pore structures.

The T_2 distribution curves of the water-saturated coal samples with different freezing temperature (10 °C, 0 °C, −10 °C, and −20 °C) obtained by using NMR are shown in Fig. 4, where the red line means the coal sample before freezing, and the black line means the coal sample after freezing. The physical properties of the coal have been tested and screened (Table 3), and the fixed carbon content (FCad) of coal sample is 88.62%, which is confirmed that the coal conforms to the high rank coal, and all coal samples are taken from the same place, whose paramagnetic mineral content have little difference, so $\rho = 0.54\times10^{-8}$ m/ms for high-rank (Xie et al., 2015; Peng et al., 2002). Based on Eq. (2) and $\rho = 0.54 \times 10^{-8}$ m/ms, the cutoff value of T_2 of the first peak is between 2 ms and 4 ms in all figures which related

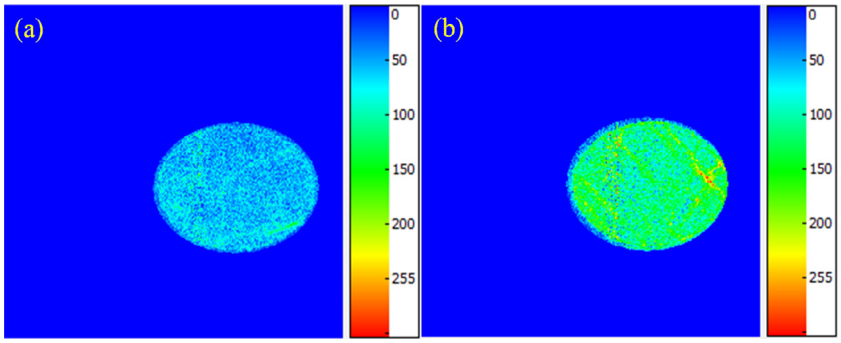

Fig. 3. MRI of water-saturated coal samples. (a - coal sample before freezing; b - coal sample after freezing.) (For interpretation of the references to color in this figure legend, the reader is referred to the web version of this article.)

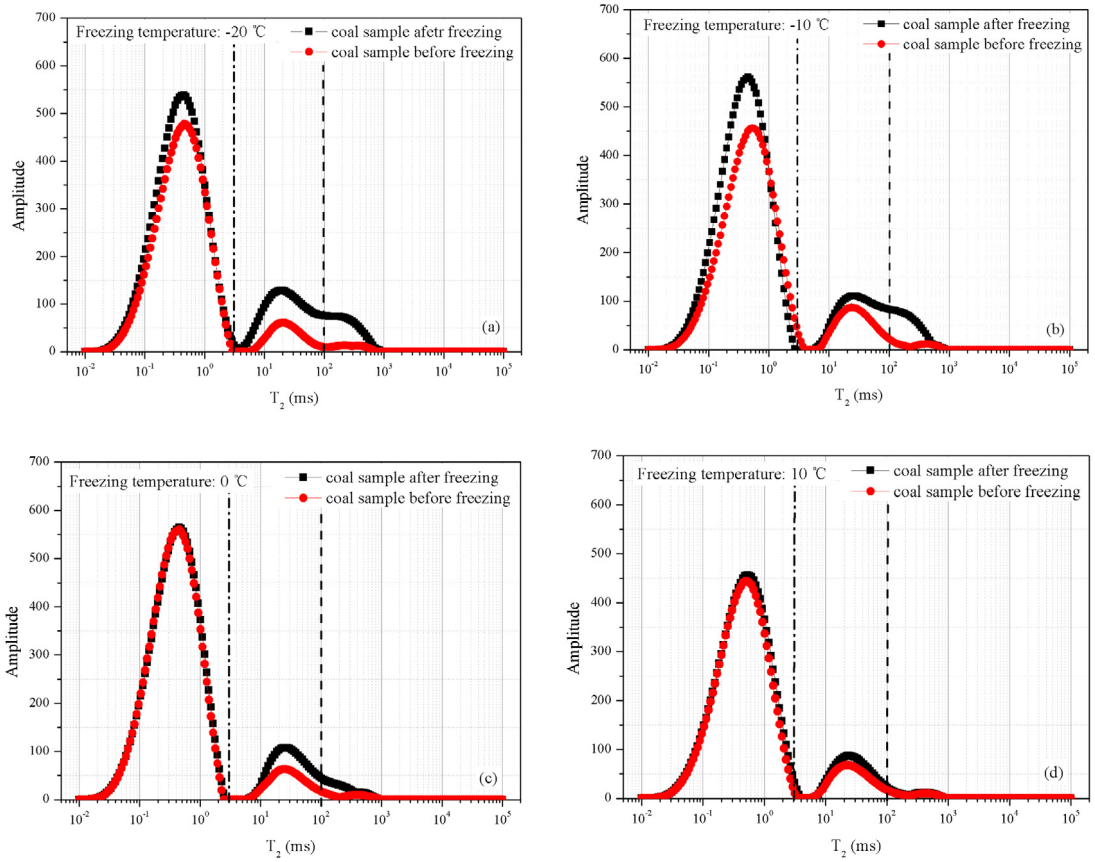

Fig. 4. Amplitudes of coal samples for different freezing temperatures. . (For interpretation of the references to color in this figure legend, the reader is referred to the web version of this article.)

to the high rank coal, which corresponds to the pores with the diameter less than 0.1 μm. The T_2 of the second peak corresponds to the pores with the diameter in the 0.1–2 μm range, and the third peak corresponds to the pores with the diameter above 2 μm. According to the classification of the coal pore diameters, as reported by Yao et al. (2010), we have attributed the first peak to micro-pores, the second peak to meso-pores, and the third peak to macro-pores and fissures. As shown in Fig. 4, the peak values appear in the order of first peak > second peak > third peak, which corresponds to the following order of coal pore abundances: micro-pores > meso-pores > macro-pores and fissures.

For coal with the same metamorphic degree and pore size, F_s and ρ can be considered as constants. And due to Eq. (1) (spherical pore, $F_s = 3$) and the first peak corresponds to the micro-pores, so it can be assumed that $C = F_s \cdot \rho$ (about 1.62×10^{-8} m/ms) based on Eq. (2); then, the equations for calculating the pore size γ_i of the T_2 distribution spectrum can be expressed as

$$\begin{aligned} \gamma_i &= C \cdot T_{2i} \quad \text{micro-pores} \\ \frac{2}{3}\gamma_i &= C \cdot T_{2i} \quad \text{meso-pores} \\ \frac{1}{3}\gamma_i &= C \cdot T_{2i} \quad \text{macro-pores and fissures} \end{aligned} \tag{3}$$

Using Eq. (3), the pore size distribution before and after freezing at different temperatures can be calculated, and the results are shown in Fig. 5. According to Chen et al. (2013), the first peak corresponds to adsorption pores (gas adsorption space), while the second and third peaks correspond to seepage pores (gas seepage

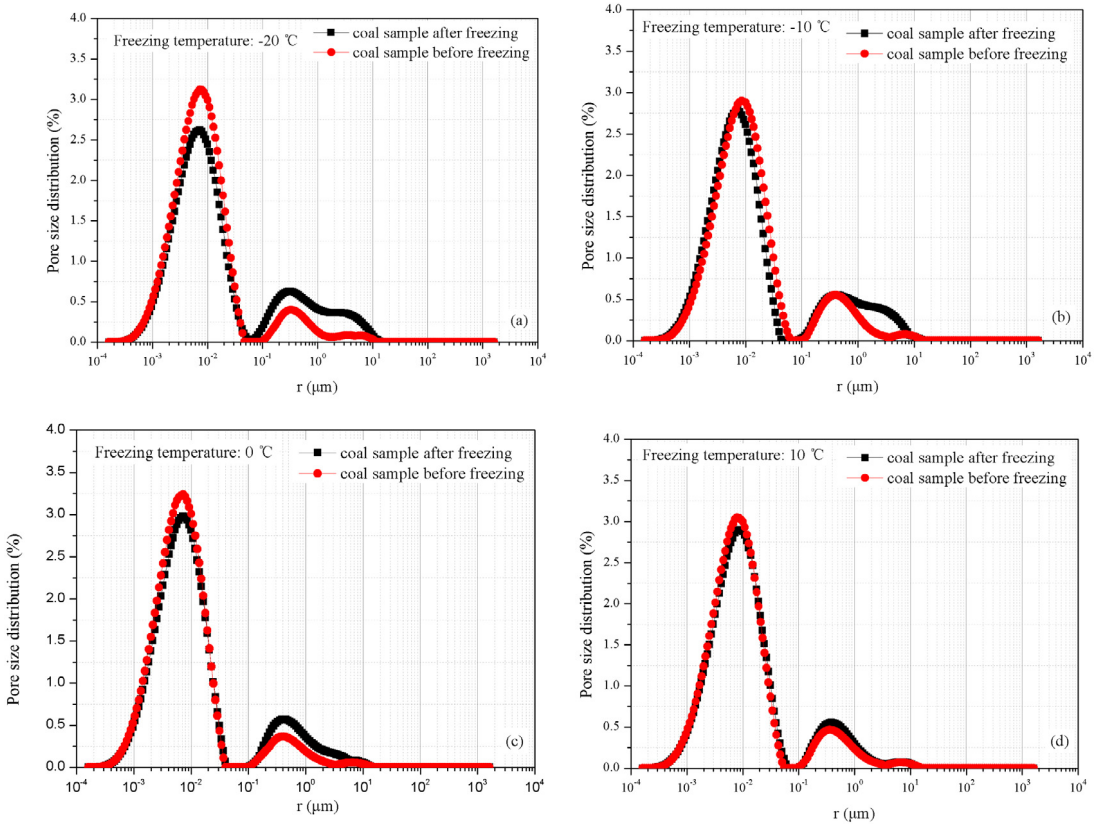

Fig. 5. Pore size distribution curves of coal samples for different freezing temperatures.

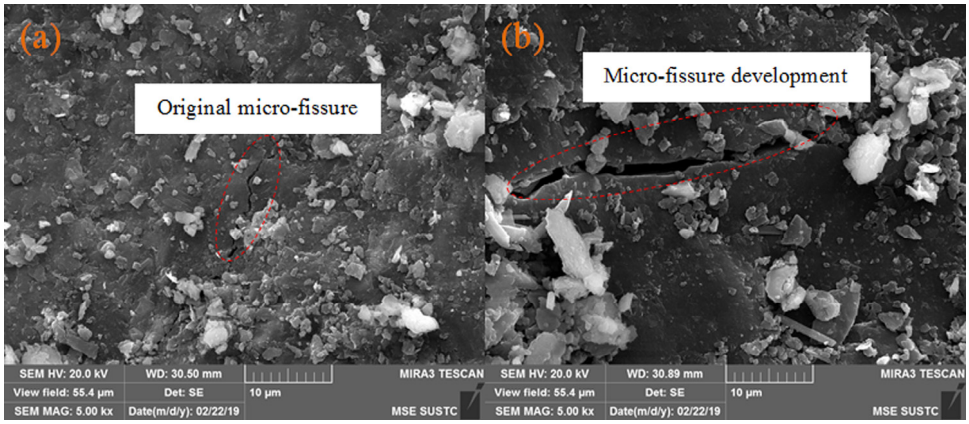

Fig. 6. SEM images of coal micro-pores. (a-coal sample before freezing; b-coal sample after freezing.)

space). It can be seen that the first peak of the pore size distribution curve corresponding to adsorption pores is lower than that before freezing, and the second and third peaks corresponding to seepage pores are higher than those before freezing. This implies that the fraction of adsorption pores decreases and the fraction of seepage pores increases. The molecular diameter of CH_4 is 0.414 nm, and most of the CH_4 in coal is adsorbed in sub-10-nm-size pores. Taking Fig. 5(d) as an example and the pore size of 10 nm as the boundary, this indicates that the proportion of sub-10-nm-size adsorption pores decreased by 1.88%; the proportion of supra-10-nm-size seepage pores increased, among which the proportion of 10–100-nm-size pores increased by 2.95% and the proportion of supra-100-nm-size pores increased by 4.83%. Seepage pores are the main factor affecting the gas diffusion and migration in coal seams; therefore, freezing significantly increases the number of gas seepage pores with pore diameter $>$ 100 nm, which can promote gas seepage in coal seams. The results show that the total porosity of coal is higher after freezing, and the number of micro-pores increases after freeze-fracturing to increase the gas adsorption capacity of the coal body. Meanwhile, the original micro-pores expand into meso-pores and macro-pores, which promotes seepage flow and increases the complexity and connectivity of coal pores, but in general reduces the proportion of adsorption pores (Fig. 6).

To quantitatively compare coal pore and crack propagation characteristics before and after freezing, based on the propagation speed of ultrasonic waves in a solid–liquid–vapor medium decreases with temperature, the ultrasonic detection method is used to measure and analyze of the speed of longitudinal waves in coal samples to determine changes in the number of pores

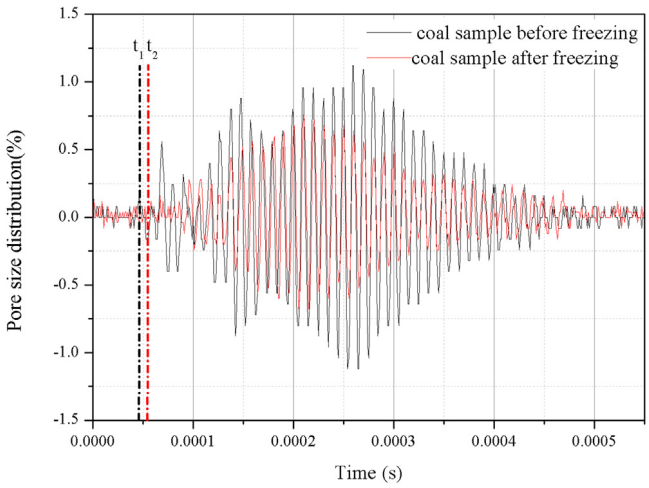

Fig. 7. Comparison of ultrasonic longitudinal wave detection in coal samples, before and after freezing.

and fissures. As the wave speed decreases, new pores and/or fissures appear in the samples. The comparison of ultrasonic P-wave detection in the coal samples before and after freezing at −20 °C is shown in Fig. 7. The ultrasound penetration time after freezing ($t_2 = 57$ μs) is longer than that before freezing ($t_1 = 45$ μs), indicating that the speed of the longitudinal wave after freeze-fracturing is lower than that before (1754.4 m/s and 2222.2 m/s, respectively), reducing by 21.1%. It is attributed to the negative correlation between freezing and the longitudinal ultrasonic wave's speed, which implies that freezing increases the number of the coal pores, while the transmission speed of the ultrasonic wave in the samples decreases.

Porosity is used for evaluating the development of coal pores; specific measures include closed porosity and connected porosity, and their values directly affect the gas quantity in the coal seam. By using the T_2 spectrum to calibrate the T_2 values of the coal samples, the porosity values for the coal samples are shown in Fig. 8. The porosity component values for each coal sample corresponding to the T_2 time after freezing increased compared with those before freezing; however, the increases in the porosity component values corresponding to the different peaks were quite different. The effect is different across different pore sizes, and it is the strongest for micro-pores. Taking a coal sample at −10 °C as an example, the sample's porosity increased from 4.26% to 5.48% owing to freezing, which corresponds to the absolute increase of 1.22% and relative increase of 28.64%. Among these, the micro-pore porosity, corresponding to the adsorption pore porosity as manifested by the first peak, increased from 3.80% to 4.69%, corresponding to the absolute increase of 0.89% and relative increase of 23.42%. The porosities of meso-pores, macro-pores, and fissures, corresponding to the seepage pore porosity as manifested by the second and third peaks, increased from 0.46% to 0.79%, corresponding to the absolute increase of 0.33% and relative increase of 71.74%. This implies that the porosity increase of seepage pores is 3.1 fold larger than that of adsorption pores; in other words, the porosities of meso-pores, macro-pores, and fissures increased more strongly than that of micro-pores.

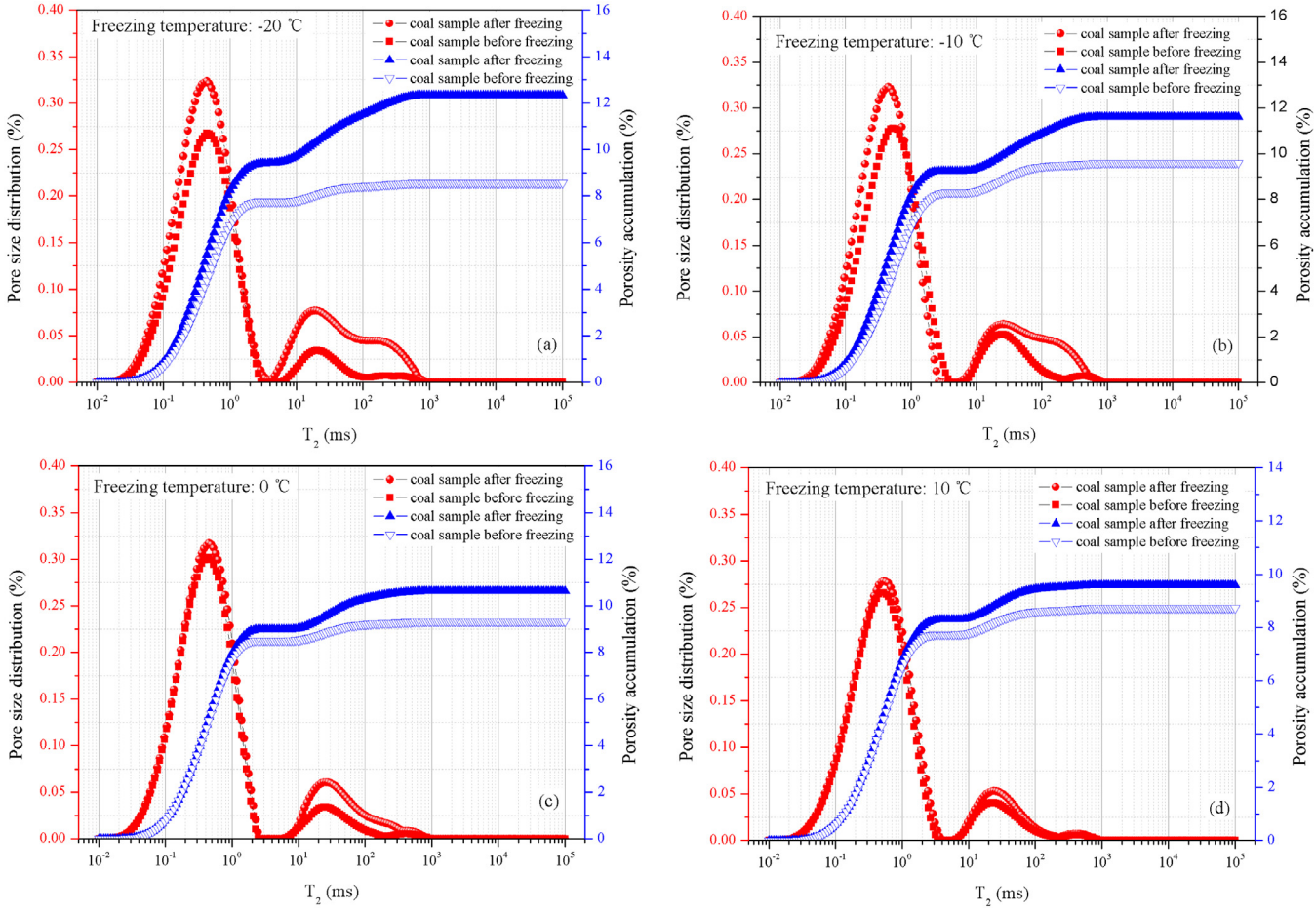

Fig. 8. Porosity curves of coal samples for different freezing temperatures.

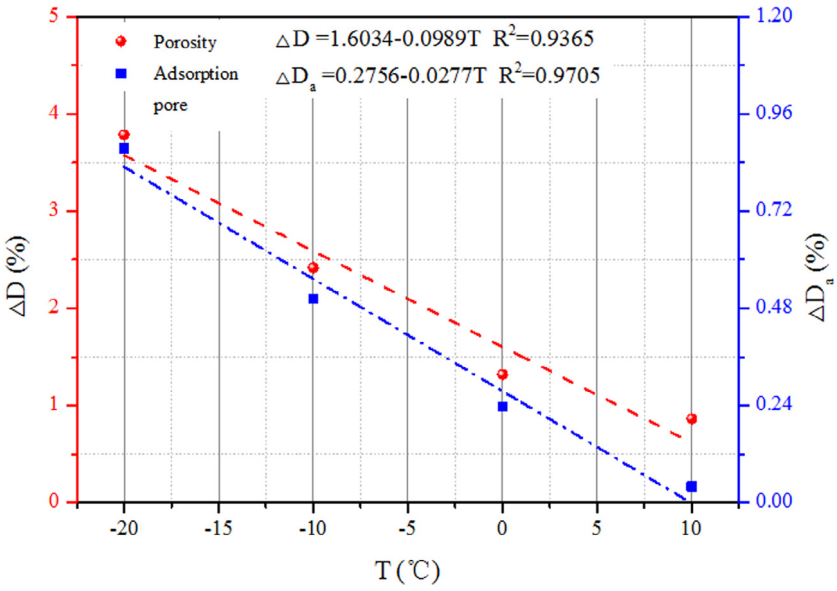

Fig. 9. Fits of porosity increment dependence on the freezing temperature in coal samples.

Compared with the porosity component representing coal sample before freezing, the T_2 values of first peak shifted to the left and the T_2 values of second and third peak shifted to the right, which shows that freezing makes the pores with smaller size and micro pores expand to the middle and large pores. Freezing increases the gas adsorption space and significantly increases the permeability and diffusion of free gas in coal, which is manifested macroscopically as the development of pores in the coal bulk.

The change in the number of coal pores can be quantitatively evaluated using the rate of change of area corresponding to the amplitude curve in the T_2 distribution spectrum, as shown in Fig. 4. Assuming that the change in the T_2 area before and after freezing is Δs, the freezing temperature is T, and the growth rate of the T_2 area is ΔD, the following equation is used:

$$\Delta D = \Delta s / s_1 = (s_2 - s_1) / s_1 \tag{4}$$

s_1—T_2 area before freezing;
s_2—T_2 area after freezing.

The area growth rate of the T_2 spectrum corresponds to the porosity increment of the corresponding coal sample. The scatter plots of porosity increment (ΔD) dependence on the freezing temperature (T) shown in Fig. 9 were generated according to the porosity increment of the coal samples at different freezing temperatures; polynomial fits and linear fits are shown as well. The correlation coefficients (R^2) are 0.94 and 0.97, respectively, suggesting that the degree of fitting strongly captures the dependence of the effective porosity increment on the freezing temperature. This implies that the number of adsorption pores and the seepage space of the coal samples increase rapidly with decreasing freezing temperature; consequently, the rate of change of the coal porosity after freeze-fracturing is positively correlated with the freezing temperature.

4.2. Moisture content dependence of pore characteristics in frozen coal samples

Fig. 10 shows the T_2 distribution spectra for the three groups of tested coal samples (water-saturated, natural, and dry), corresponding to different moisture contents (4.45%, 1.90%, and 0%); the freezing temperature was −20 °C.

As shown in Fig. 10, the order of the T_2 curve amplitudes is: water-saturated coal sample > natural coal sample > dry coal sample, which means the T_2 curve amplitude increases with increasing moisture content, and the higher the moisture content of the coal samples, the stronger the increase. Regarding the pore size distributions of the tested coal samples, with increasing moisture content, the seepage space in the frozen coal increases, which indicates that freeze-fracturing can promote formation of new pores and fissures, open closed pores, and connect coal fissures.

Regarding the coal pore structure, water molecules (diameter, ~0.4 nm) are easily adsorbed on the coal pore surface, and water molecules absorbed by micro-pores or coal matrix cannot be completely removed using centrifugal dehydration or vacuum drying. Thus, the porosity measured based on the NMR imaging of the T_2 spectrum is the residual porosity (depicted by the red curve in Fig. 11). The blue curve in Fig. 11 is the cumulative coal porosity, and it should be subtracted from the residual porosity to obtain the effective porosity. In addition, the effective porosity increases with increasing moisture content in the tested coal samples.

The tested coal samples exhibited different pore changes after freezing, but a majority of them displayed an increase in porosity with increasing moisture content. According to this, the scatter plots of the porosity change (ΔD) dependence on the moisture content (W) were generated, and the scatter data were fitted using polynomial and linear fits, as shown in Fig. 12. The correlation coefficients R^2 for the polynomial and linear fits using the ΔD equation were 0.9171 and 0.9673, respectively. This suggests that polynomial fits accurately captured the dependence of the porosity increment (ΔD) on the moisture content (W). These results indicate that the number of adsorption pores and the seepage space in the tested coal samples increased rapidly with increasing moisture content, and the porosity change rate of frozen coal was positively correlated with the moisture content.

4.3. Coal permeability changes under freeze-fracturing

Coal permeability is an important index for evaluating gas production in coal seams since it reflects the gas flow ability, and is closely related to the distribution and connectivity of cores.

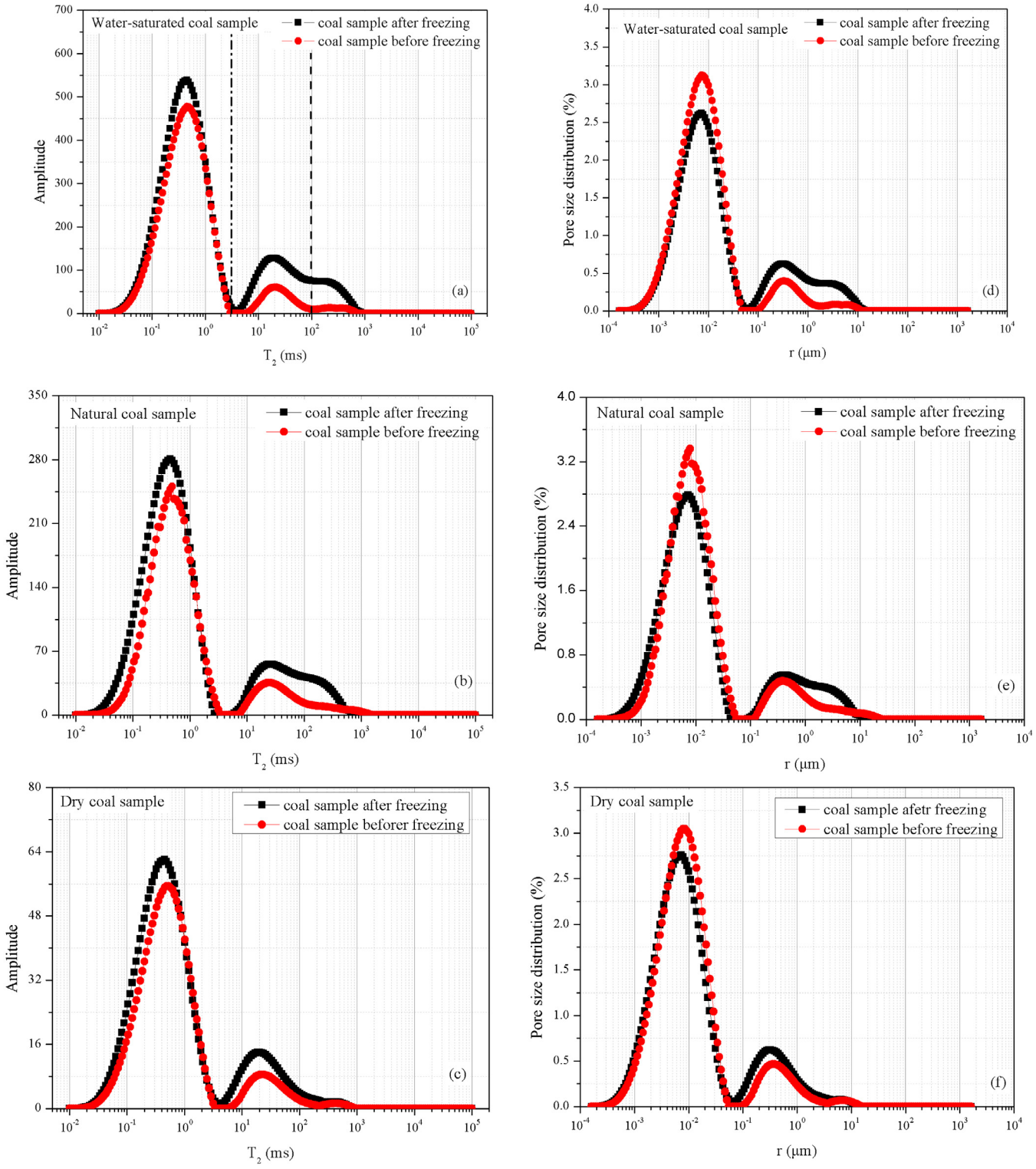

Fig. 10. Amplitude and pore size distributions for coal samples with different moisture content.

Porosity and pore size distribution curve of the T_2 spectrum can be used to calculate permeability. Yao et al. (2010) established a permeability calculation model based on NMR, using the porosity of water-saturated coal samples:

$$k = 0.49 \times EXP\,(\varphi/1.35) - 0.54 \tag{5}$$

k—permeability of coal sample, mD;
φ—total coal porosity, %.

Using this model, the permeability of water-saturated coal samples was calculated and plotted in Fig. 13, for different freezing temperatures. The fit correlation coefficient R^2 is 0.8472, suggesting that the polynomial fit is able to accurately capture the dependence of the sample permeability on the freezing temperature T. Conclusions could be made that the coal permeability after freezing increases exponentially with its porosity, and permeabil-

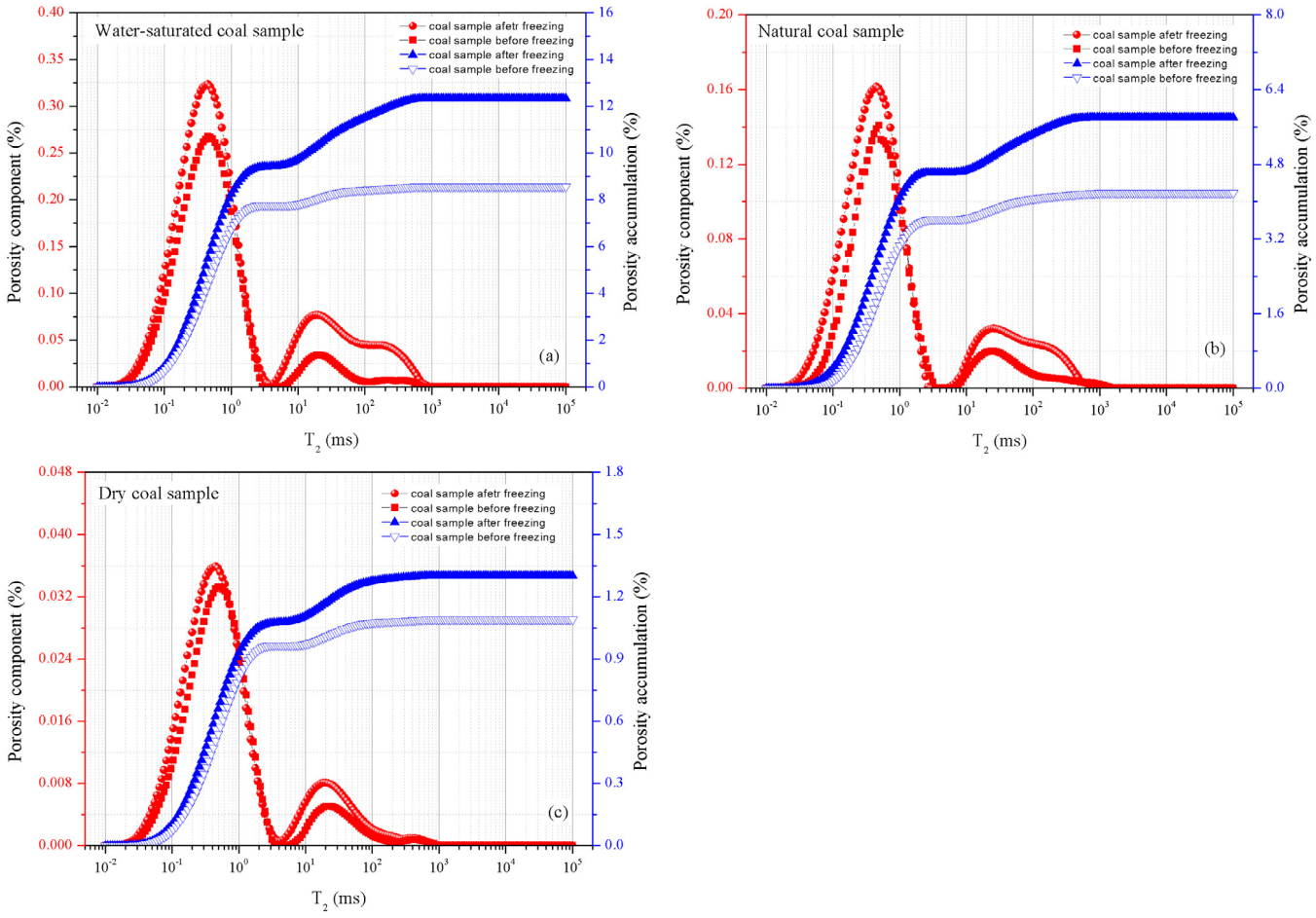

Fig. 11. Porosity curves of coal samples with different moisture content. . (For interpretation of the references to color in this figure legend, the reader is referred to the web version of this article.)

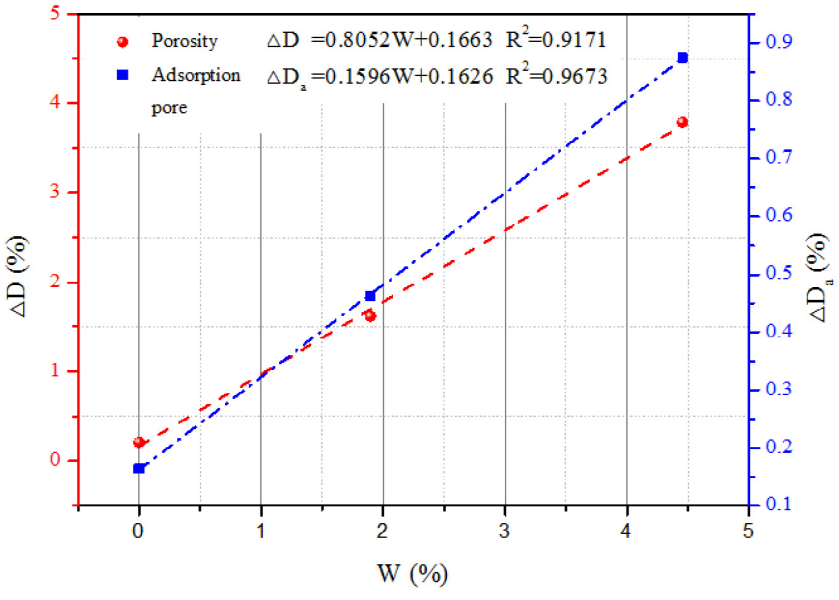

Fig. 12. Fit of porosity increment dependence on the moisture content for frozen coal samples.

ity of frozen coal samples is higher than that before freezing. This confirms that freezing changes the pore structure and promotes the pore expansion of coal samples, thus increasing the seepage space of coal samples, increasing their permeability.

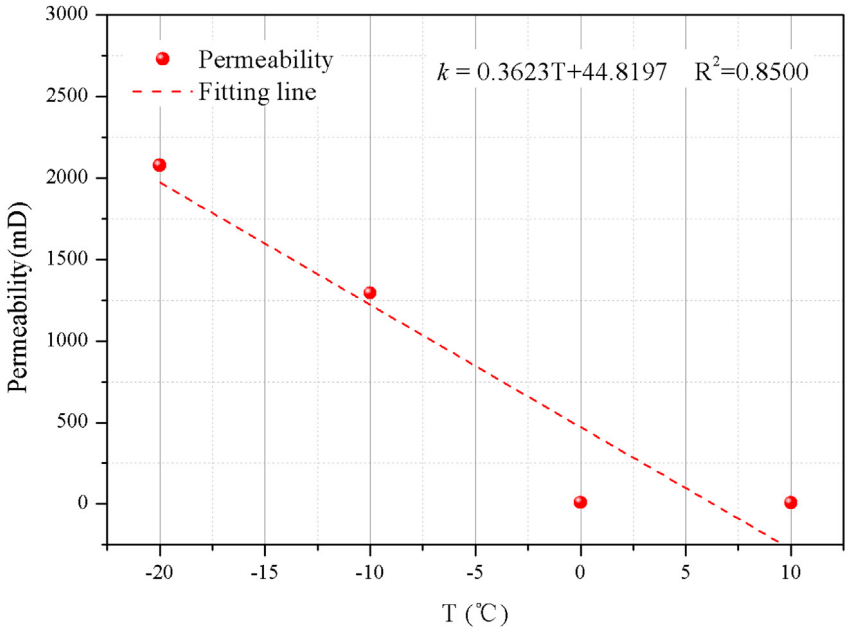

Fig. 13. Fit of permeability dependence on the freezing temperature for water-saturated coal sample.

5. Conclusion

To study the effect of freeze-fracturing on coal pore characteristics, coal samples under different freezing temperatures and moisture content levels are analyzed by studying the T_2 spectra obtained from NMR. The studies addressed pore type classification, pore evolution, and porosity observations in frozen coal samples. As research shows, freeze-fracturing promotes the development of coal pores and fissures, increases the pore size and number of adsorption pores and seepage pores, and makes pore structures more complex. The porosity change rate of frozen coal is positively correlated with freezing temperature, and freezing significantly increases the gas seepage pore for pore diameters $>$ 100 nm, which can promote gas seepage in coal. The speed of the longitudinal ultrasonic wave is negatively correlated with freezing; that is, freezing increases the abundance of pores and cracks in the coal body, and then slows down the transmission speed of ultrasonic waves in specimens. The porosity change rate of frozen coal is positively correlated with water content; that is, the number of adsorption pores and seepage space in coal samples increases rapidly with increasing water content. Freeze-fracturing affects the pore distribution characteristics of coal samples, which promotes the opening of closed pores and the connection between cracks in the coal body, and makes use of gas seepage and diffusion in the coal body. The permeability is straightly correlated with freezing temperature T, which confirms that the permeability of frozen coal increases linearly with porosity. By using the computational model of porosity and permeability, it is concluded that freeze-fracturing can play a role in coal seam seepage.

Acknowledgments

This work is financially supported by the National Key Research and Development Program, China (Grant No. 2017YFC0804202), the Science and Technology Research Program of Chongqing Municipal Education Commission, China (Grant No. KJQN201800117 and KJQN201800115), and funded by the Open Research Fund Program (No. E21820) of Hunan Provincial Key Laboratory of Shale Gas Resource Utilization (Hunan University of Science and Technology), China, all are gratefully acknowledged. The authors also thank the editor and anonymous reviewers for their valuable advice.

References

Brown, R., Fatt, I., 1956. Measurements of fractional wettability of oil field rocks by the nuclear magnetic relaxation method. Trans. AIME 207, 262–264. http://dx.doi.org/10.2523/743-G.

Cai, T., Feng, Z., Jiang, Y., Zhao, D., 2019. Thermodynamic characteristics of methane adsorption of coal with different initial gas pressures at different temperatures. Adv. Mater. Sci. Eng. 2019, 1–9. http://dx.doi.org/10.1155/2019/4751209.

Cai, C., Gao, F., Yang, Y., 2018. The effect of liquid nitrogen cooling on coal cracking and mechanical properties. Energy Explor. Exploit. 36, 1609–1628. http://dx.doi.org/10.1177/0144598718766630.

Chen, X., Liu, J., Wang, L., Qi, L., 2013. Influence of pore size distribution of different metamorphic grade of coalon adsorption constant. J. China Coal Soc. 38, 294–300. http://dx.doi.org/10.13225/j.cnki.jccs.2013.02.025.

Chen, J., Peng, H., Fan, J., 2020. Microscopic investigations on the healing and softening of damaged salt by uniaxial deformation from CT, SEM and NMR: effect of fluids (brine and oil). RSC Adv. 10, 2877–2886. http://dx.doi.org/10.1039/C9RA05866D.

Chen, S., Tang, D., Tao, S., Ji, X., Xu, H., 2019. Fractal analysis of the dynamic variation in pore-fracture systems under the action of stress using a low-field NMR relaxation method: An experimental study of coals from western Guizhou in China. J. Petrol Sci. Eng. 173, 617–629. http://dx.doi.org/10.1016/j.petrol.2018.10.046.

Dai, S., Yan, X., Ward, C.R., Hower, J.C., Zhao, L., Wang, X., Zhao, L., Ren, D., Finkelman, R.B., 2018. Valuable elements in chinese coals: a review. Int. Geol. Rev. 60, 590–620. http://dx.doi.org/10.1080/00206814.2016.1197802.

Deng, J., Xu, Y., Jiang, H., Hu, S., 2013. Safe and effective production of coal mine promoted by coalbed methane reclamation. Adv. Mater. Res. 310, 616–618. http://dx.doi.org/10.4028/www.scientific.net/AMR.616-618.310.

Goraya, N.S., Rajpoot, N., Sivagnanam, B.M., 2019. Coal bed methane enhancement techniques: A review. ChemistrySelect 4, 3585–3601. http://dx.doi.org/10.1002/slct.201803633.

Guo, R., Kantzas, A., 2009. Assessing the water uptake of alberta coal and the impact of CO_2 injection with low-field NMR. J. Can. Pet. Technol. 48, 40–46. http://dx.doi.org/10.2118/09-07-40.

Guo, R., Mannhardt, K., Kantzas, A., 2007. Characterizing moisture and gas content of coal by low-field NMR. J. Can. Pet. Technol. 46, 49–54. http://dx.doi.org/10.2118/2006-022.

Javadpour, F., McClure, M., Naraghi, M.E., 2015. Slip-corrected liquid permeability and its effect on hydraulic fracturing and fluid loss in shale. Fuel 160, 549–559. http://dx.doi.org/10.1016/j.fuel.2015.08.017.

Ko, D., 2018. Development of a dynamic simulation model of a hollow fiber membrane module to sequester CO_2 from coalbed methane. J. Membr. Sci. 546, 258–269. http://dx.doi.org/10.1016/j.memsci.2017.09.040.

Li, L., Peng, J., Gao, Q., Sun, M., Liu, Y., Li, M., Chen, B., Bo, K., 2016. Pressure retaining method based on phase change for coring of gas hydrate-bearing sediments in offshore drilling. Appl. Therm. Eng. 107, 633–641. http://dx.doi.org/10.1016/j.applthermaleng.2016.06.174.

Li, L., Tan, J., Wood, D.A., Zhao, Z., Becker, D., Lyu, Q., Shu, B., Cheng, H., 2019. A review of the current status of induced seismicity monitoring for hydraulic fracturing in unconventional tight oil and gas reservoirs. Fuel 242, 195–210. http://dx.doi.org/10.1016/j.fuel.2019.01.026.

Liang, Y., Dai, J., Zou, Q., Li, L., L, Y., 2019. Ignition mechanism of gas in goaf induced by the caving and friction of sandstone roof containing pyrite. Process Saf. Environ. Prot. http://dx.doi.org/10.1016/j.psep.2019.02.005.

Liu, J., Feng, X., Wang, D., 2019. Determination of water content in crude oil emulsion by LF-NMR CPMG sequence. Petrol Sci. Technol. 37, 1123–1135. http://dx.doi.org/10.1080/10916466.2019.1578795.

Liu, X., Wu, C., 2017. Simulation of dynamic changes of methane state based on NMR during coalbed methane output. Fuel 194, 188–194. http://dx.doi.org/10.1016/j.fuel.2017.01.011.

Ni, X., Li, Q., Wang, Y., Gao, S., 2015. Permeability variation characteristics of coal after injecting carbon dioxide into a coal seam. Int. J. Min. Sci. Technol. 25, 665–670. http://dx.doi.org/10.1016/j.ijmst.2015.05.022.

Peng, S., Wei, Z., Guan, Z., 2002. Experimental study of impact of paramagnetic materials to the nuclear magnetic relaxation characteristics of rocks. Geophys. Prospect. Pet. 3, 372–376.

Shi, X., Pan, J., Hou, Q., Jin, Y., Wang, Z., Niu, Q., Li, M., 2018. Micrometer-scale fractures in coal related to coal rank based on micro-CT scanning and fractal theory. Fuel 212, 162–172. http://dx.doi.org/10.1016/j.fuel.2017.09.115.

Shikhov, I., Li, R., Arns, C.H., 2018. Relaxation and relaxation exchange NMR to characterise asphaltene adsorption and wettability dynamics in siliceous systems. Fuel 220, 692–705. http://dx.doi.org/10.1016/j.fuel.2018.02.059.

Sun, Z., Shi, J., Wu, K., Liu, W., Wang, S., Li, X., 2019a. A prediction model for desorption area propagation of coalbed methane wells with hydraulic fracturing. J. Petrol Sci. Eng. 175, 286–293. http://dx.doi.org/10.1016/j.petrol.2018.12.047.

Sun, Y., Zhai, C., Qin, L., Xu, J., Yu, G., 2018. Coal pore characteristics at different freezing temperatures under conditions of freezing-thawing cycles. Environ. Earth Sci. 77, http://dx.doi.org/10.1007/s12665-018-7693-y.

Sun, Y., Zhao, Y., Yuan, L., 2019b. Impact of coal composition and pore structure on gas adsorption: a study based on a synchrotron radiation facility. Greenh. Gases-Sci. Technol. http://dx.doi.org/10.1002/ghg.1935.

Wang, F., Luo, Y., Liang, Y., Peng, J., Li, B., 2019. Sampling methane-bearing coal seams by freezing method: coalbed methane desorption and inhibition characteristics under freezing temperature. Nat. Resour. Res. http://dx.doi.org/10.1007/s11053-019-09488-3.

Wen, H., Wei, G., Ma, L., Li, Z., Lei, C., Hao, J., 2019. Damage characteristics of coal microstructure with liquid CO_2 freezing-thawing. Fuel 249, 169–177. http://dx.doi.org/10.1016/j.fuel.2019.03.110.

Xie, S., Yao, Y., Chen, J., Yao, W., 2015. Research of micro-pore structure in coal reservoir using low-field NMR. J. China Coal Soc. 40, 170–176. http://dx.doi.org/10.13225/j.cnki.jccs.2014.0755.

Xu, J., Zhai, C., Liu, S., Qin, L., Wu, S., 2017. Pore variation of three different metamorphic coals by multiple freezing-thawing cycles of liquid CO_2 injection for coalbed methane recovery. Fuel 208, 41–51. http://dx.doi.org/10.1016/j.fuel.2017.07.006.

Yang, M., Bi, J., 2018. Influence of extreme temperature on the pore and fracture development of high-rank coal. Adv. Civ. Eng. http://dx.doi.org/10.1155/2018/4529751.

Yao, Y., Liu, D., Che, Y., Tang, D., Tang, S., Huang, W., 2010. Petrophysical characterization of coals by low-field nuclear magnetic resonance (NMR). Fuel 89, 1371–1380. http://dx.doi.org/10.1016/j.fuel.2009.11.005.

Yin, G., Shang, D., Li, M., Huang, J., Gong, T., Song, Z., Deng, B., Liu, C., Xie, Z., 2018. Permeability evolution and mesoscopic cracking behaviors of liquid nitrogen cryogenic freeze fracturing in low permeable and heterogeneous coal. Powder Technol. 325, 234–246. http://dx.doi.org/10.1016/j.powtec.2017.10.058.

Yoon, S.Y., Choi, B.S., Ahn, J.H., Kim, T.S., 2019. Improvement of integrated gasification combined cycle performance using nitrogen from the air separation unit as turbine coolant. Appl. Therm. Eng. 151, 163–175. http://dx.doi.org/10.1016/j.applthermaleng.2019.01.110.

Zhai, C., Qin, L., Liu, S., Xu, J., Tang, Z., Wu, S., 2016. Pore structure in coal: Pore evolution after cryogenic freezing with cyclic liquid nitrogen injection and its implication on coalbed methane extraction. Energy Fuel 30, 6009–6020. http://dx.doi.org/10.1021/acs.energyfuels.6b00920.

Zhai, C., Wu, S., Liu, S., Qin, L., Xu, J., 2017. Experimental study on coal pore structure deterioration under freeze-thaw cycles. Environ. Earth Sci. 76, http://dx.doi.org/10.1007/s12665-017-6829-9.

Zhang, S., Huang, Z., Wang, H., Zhang, H., Zhang, C., Xiong, C., 2018a. Thermal characteristics analysis with local thermal non-equilibrium model during liquid nitrogen jet fracturing for HDR reservoirs. Appl. Therm. Eng. 143, 482–492. http://dx.doi.org/10.1016/j.applthermaleng.2018.07.088.

Zhang, P., Lu, S., Li, J., Chen, C., Xue, H., Zhang, J., 2018b. Petrophysical characterization of oil-bearing shales by low-field nuclear magnetic resonance (NMR). Mar. Pet. Geol. 89, 775–785. http://dx.doi.org/10.1016/j.marpetgeo.2017.11.015.

Zhao, Y., Sun, Y., Liu, S., Chen, Z., Yuan, L., 2018. Pore structure characterization of coal by synchrotron radiation nano-CT. Fuel 215, 102–110. http://dx.doi.org/10.1016/j.fuel.2017.11.014.

Zhao, H., Wang, X., Liu, Z., 2019. Experimental investigation of hydraulic sand fracturing on fracture propagation under the influence of coal macrolithotypes in hancheng block, China. J. Petrol Sci. Eng. 175, 60–71. http://dx.doi.org/10.1016/j.petrol.2018.12.031.

Zheng, S., Yao, Y., Liu, D., Cai, Y., Liu, Y., 2018. Characterizations of full-scale pore size distribution, porosity and permeability of coals: a novel methodology by nuclear magnetic resonance and fractal analysis theory. Int. J. Coal Geol. 196, 148–158. http://dx.doi.org/10.1016/j.coal.2018.07.008.